Atmos. Chem. Phys. Discuss., https://doi.org/10.5194/acp-2018-142
Manuscript under review for journal Atmos. Chem. Phys.
Discussion started: 27 March 2018

Atmospheric Chemistry and Physics Discussions
Open Access

A statistical examination of the effects of stratospheric sulphate geoengineering on tropical storm genesis

Qin Wang[1], John C. Moore[1,2,3*], Duoying Ji[1]

[1] College of Global Change and Earth System Science, Beijing Normal University, 19 Xinjiekou Wai St., Beijing, 100875, China

[2] Arctic Centre, University of Lapland, P.O. Box 122, 96101 Rovaniemi, Finland

[3] CAS Center for Excellence in Tibetan Plateau Earth Sciences, Beijing 100101, China

*** *Correspondence to*: John C. Moore. College of Global Change and Earth System Science Beijing Normal University 19 Xinjiekou Wai street, Beijing,China,100875 fax:+86-1058802165 Mobile +86-13521460942 E-mail: john.moore.bnu@gmail.com.**

Atmos. Chem. Phys. Discuss., https://doi.org/10.5194/acp-2018-142
Manuscript under review for journal Atmos. Chem. Phys.
Discussion started: 27 March 2018

Abstract

The thermodynamics of the ocean and atmosphere partly determine variability in tropical cyclone (TC) number and intensity and are readily accessible from climate model output, but a complete description of TC variability requires much more dynamical data than climate models can provide at present. Genesis potential index (GPI) and ventilation index (VI) are combinations of potential intensity, vertical wind shear, relative humidity, midlevel entropy deficit, and absolute vorticity that can quantify both thermodynamic and dynamic forcing of TC activity under different climate states. Here we use six CMIP5 models that have run the RCP4.5 experiment and the Geoengineering Model Intercomparison Project (GeoMIP) stratospheric aerosol injection G4 experiment, to calculate the two TC indices over the 2020 to 2069 period across the 6 ocean basins that generate tropical cyclones. Globally, GPI under G4 is lower than under RCP4.5, though both have a slight increasing trend. Spatial patterns in the effectiveness of geoengineering show reductions in TC in the North Atlantic basin, and Northern Indian Ocean in all models except NorESM1-M. In the North Pacific, most models also show relative reductions under G4. Most models project potential intensity and relative humidity to be the dominant variables affecting genesis potential. Changes in vertical wind shear are significant, but both it and vorticity exhibit relatively small changes with large variation across both models and ocean basins. We find that tropopause temperature is not a useful addition to sea surface temperature in projecting TC genesis, despite radiative heating of the stratosphere due to the aerosol injection, and heating of the upper troposphere affecting static stability

Atmos. Chem. Phys. Discuss., https://doi.org/10.5194/acp-2018-142
Manuscript under review for journal Atmos. Chem. Phys.
Discussion started: 27 March 2018

and potential intensity. Thus, simplified statistical methods that quantify the thermodynamic state of the major genesis basins may reasonably be used to examine stratospheric aerosol geoengineering impacts on TC activity.

Key word: tropical cyclone, hurricanes, ENSO, statistical methods

1 Introduction

Anthropogenic greenhouse gases emission are changing climate (IPCC, 2007). The best solution for limiting climate change is to reverse the growth in net greenhouse gases emissions. It is doubtful that reductions in emission can be done fast enough to limit global mean temperatures rises to targets such as the 1.5° or 2°C pledged at the Paris climate meeting (Rogelj et al., 2015). Geoengineering is the deliberate and large-scale intervention of Earth's climate system to retard climate warming (Crutzen, 2006; Wigley, 2006). Geoengineering by solar radiation management (SRM) attempts to lessen the incoming sunlight to counteract the effect of global warming. The Geoengineering Model Intercomparison Project (GeoMIP) (Kravitz, et al.,2011) is a standardized set of experiments designed to facilitate earth system model (ESM) simulations of geoengineered climates, and is supported by about 12 model groups globally, with further experiments planned under CMIP6 (Kravitz et al., 2015). Climate system thermodynamics will certainly change under SRM geoengineering where the reduction in short wave radiation is designed to offset increases in long wave absorption (Huneeus et al., 2014).

Atmos. Chem. Phys. Discuss., https://doi.org/10.5194/acp-2018-142
Manuscript under review for journal Atmos. Chem. Phys.
Discussion started: 27 March 2018

Tropical cyclones (TCs) are one of the most disastrous weather phenomena influencing agriculture, human life, and property (Chan et al., 2005). The large-scale changes in surface temperatures under greenhouse gas forcing will impact cyclogenesis changing both the frequency and intensity of tropical cyclones (Grinsted et al., 2012; 2013). Hence, how tropical cyclones would change in a geoengineered world is of general as well as scientific interest for its enormous social and economic impact. However, since almost all climate models do not, at present, possess the resolution required to simulate directly the response of tropical cyclones to changing patterns of radiative forcing, methods that rely on the statistical links between the thermodynamics of the ocean and atmosphere with cyclone dynamics have been the topic of studies.

Many methods have used to study the changes in typhoons under climate warming. Some focus on the movement of tropical storm tracks, tropical cyclone intensity and frequency by downscaling (Emanuel, 2006). The most direct way is to use historical climate and storm records to quantitatively study tropical cyclone activity and its relation to key variables such as local, tropical and global sea surface temperatures, and various teleconnection patterns (Grinsted et al., 2012; Emanuel, 2008; Landsea, 2005; Gray, 1979). Potential intensity theory (Bister et al., 1998; Emanuel et al., 2004) predicts the dependence of typhoon wind speed on the air-sea thermodynamic imbalance and the temperature of the lower stratosphere. For example, many studies suggest that wind shear has inhibitory effect on the TC activity (Vecchi et al., 2007). Others have also identified changes in the large-scale environmental factors influencing the tropical storm activity to assess the TC activities in the future (Tippett et al., 2011; Grinsted et al., 2013).

While much is known about which factors influence genesis, a quantitative theory is lacking, so empirical methods have been used to define the relationship between large-scale environmental factors and tropical cyclogenesis. The GPI uses four environmental variables: potential intensity, low-level absolute vorticity, vertical wind shear, and relative humidity. Tang et al. (2012) introduced the VI, defined as the flux of low-entropy air into a tropical disturbance or TC, because ventilation disrupts the formation of a deep, moist column that is hypothesized to be necessary for the spin up of the vortex (Bister et al., 1997; Nolan, 2007; Rappin et al., 2010). For the Atlantic hurricane region, Tippett et al. (2011) formulated a genesis potential index using the relative sea surface temperature, defined as the tropical Atlantic sea surface temperatures minus the tropical mean sea surface temperatures, and midlevel relative humidity in lieu of the potential intensity and non-dimensional entropy deficit, respectively. Dynamic potential intensity (DPI) is yet another index designed to describe the ocean's impact on tropical cyclones (Balaguru et al., 2015). These indices represent the climatological thermodynamic spatial and seasonal control of TC genesis and not the dynamic development of individual storms, which is more or less beyond the abilities of contemporary climate models. The relative contribution of the individual large-scale environmental factors to TC genesis may be different in different ocean basins (Wang et al., 2012).

An increase in future global TC frequency has been projected based on dynamical downscaling CMIP5 models (Emanuel, 2013). However, the same downscaling applied to the CMIP3 models projected a decrease in global TC frequency (Tory et al., 2013; Emanuel et al., 2006). Some models show that although Atlantic TC frequency will decrease, the frequency of severe TC will increase, and different TC basins are predicted to behave differently (Emanuel et al., 2008; Thomas et al., 2015; Kang et al., 2012).

There has been little research about TC changes under geoengineering. Moore et al. (2015) used statistical relation between Atlantic tropical storm surges and spatial patterns of global surface temperature to deduce that moderate amounts of SRM could reduce the frequency of the most intense hurricanes relative to greenhouse gas only climates. Jones et al. (2017) show that applying aerosol injection to northern and southern hemispheres separately reduced the numbers of TC in North Atlantic if the northern hemisphere was cooled, while increasing them if aerosol was released only in the southern hemisphere, relative to both greenhouse gas forcing both with, and without, global stratospheric aerosol injection.

Here we examine ESM simulations of global TC evolution under stratospheric sulphate injection geoengineering and greenhouse gas forcing based on the climatological GPI and VI. We explore the effects of geoengineering on TC thermodynamics, and study regional characteristics of typhoon and hurricane development after implementation of geoengineering.

Atmos. Chem. Phys. Discuss., https://doi.org/10.5194/acp-2018-142
Manuscript under review for journal Atmos. Chem. Phys.
Discussion started: 27 March 2018

Section 2 introduces the methods and data used in this study. Section 3 describes the temporal and spatial variations of the GPI and ventilation index in six models, in greenhouse gas and SRM simulations. We quantify the contribution of each variable to TC genesis using two statistical methods. Finally we study the effect of ENSO on TC and TC track of HadGEM2-ES model. A discussion and conclusions are provided in section 4.

2 Methods and data

a. Methods

We use climate model output from the GeoMIP G4 experiment (Kravitz et al., 2011) and the control simulation, RCP4.5 experiment of CMIP5 (Taylor et al., 2012) to analysis the characteristic of TC changes in the future in different models. G4 is based on the greenhouse gas emissions from the RCP4.5 scenario but short wave radiative forcing is reduced by injection of SO_2 into the equatorial lower stratosphere at a rate of 5 Tg per year from the year 2020 to 2069. The experiment continues for a further 20 years to 2089 with only greenhouse gas forcing as specified by RCP4.5. The general climate response to G4 forcing has been discussed by Yu et al. (2015). Between 2050 and 2069, global surface air temperatures warm by 1.3 ℃ in RCP4.5, and by 0.79 ℃ with G4 relative to 2010–2029. Over the same interval, tropical North Atlantic temperatures in the so-called Main Development Region (MDR) of cyclogenesis in the

Atmos. Chem. Phys. Discuss., https://doi.org/10.5194/acp-2018-142
Manuscript under review for journal Atmos. Chem. Phys.
Discussion started: 27 March 2018

basin warm by 0.8 ℃ and 0.4 ℃ with RCP4.5, and G4, respectively (Moore et al., 2015).

We assess the large-scale environmental conditions for TC generation primarily in reference to the widely used genesis potential and ventilation index (GPI), and use results for the VI for comparison. While other indices also exist as mentioned above, the data fields required to calculate them are presently not all available. The signal to noise ratio of the G4 experiment is not as large as that of G1 (Yu et al., 2015) where solar dimming offsets quadrupled CO_2 concentrations. It is, however, more interesting for TC studies because the sulphate aerosol injected into the stratosphere causes radiative heating that will potentially affect the deep tropospheric convention systems that characterize intense tropical storms.

The GPI has been widely employed to represent TC activities (e.g., Song et al., 2015). We use the Emanuel et al., (2004) method to calculate the GPI as follows:

$$GPI = \left|10^5 \eta\right|^{3/2} \left(\frac{H}{50}\right)^3 \left(\frac{V_{pot}}{70}\right)^3 \left(1 + 0.1 V_{shear}\right)^{-2} \quad (1)$$

where η is the absolute vorticity in s^{-1}, H is the relative humidity at 700 hPa in percent, V_{pot} is the Potential intensity in ms^{-1}, and V_{shear} is the magnitude of the vector shear from 850 to 200 hPa, in ms^{-1}. Potential intensity (Emanuel, 2000) is defined as

$$V_{pot}^2 = C_p \left(T_S - T_O\right) \frac{T_S}{T_O} \frac{C_K}{C_D} \left(\ln \theta_e^* - \ln \theta_e\right) \quad (2)$$

Atmos. Chem. Phys. Discuss., https://doi.org/10.5194/acp-2018-142
Manuscript under review for journal Atmos. Chem. Phys.
Discussion started: 27 March 2018

Where T_S is the ocean surface temperature, T_O is the mean outflow temperature, which is taken near the tropopause at the 100 hPa level and spatially averaged, C_K is the exchange coefficient for enthalpy, and C_D is the drag coefficient. θ_e^* is the saturation equivalent potential temperature at the ocean surface, and θ_e is the boundary layer equivalent potential temperature.

We also use a second and more recent method to estimate TC called the ventilation index (Tang, et al., 2014), defined as:

$$VI = \frac{\chi_m V_{shear}}{V_{pot}} \quad (3)$$

Where χ_m is the (nondimensional) entropy deficit, defined as:

$$\chi_m = \frac{s_m^* - s_m}{s_{SST}^* - s_b} \quad (4)$$

where s_m^* is the saturation entropy at 600 hPa in the inner core of the TC, s_m is the environmental entropy at 600 hPa, s_{SST}^* is the saturation entropy at the sea surface temperature, and s_b is the entropy of the boundary layer, which we chose as the 925 hPa layer. The numerator of (4) is the difference in entropy between the TC and the environment at mid-levels, while the denominator is the air-sea disequilibrium, both are calculated following Emanuel (1994).

b. Data

Although to date 8 ESM have performed the greenhouse gas and G4 simulations, we selected a subset of 6 models to use here based on access to all required model data fields (Table 1). We use monthly sea surface temperature (SST), relative humidity, vertical wind shear, sea level pressure, specific humidity, air temperature. All the model outputs at different spatial resolutions were interpolated to a common grid (128×64) using the bilinear interpolation method. All the models were weighted equally in the ensemble mean, so the models with more than a single ensemble member were first averaged before taking the overall model ensemble mean.

c. TC basins

Factors influencing TC change are diverse across different ocean basins. Some researchers (Emanuel, 2010; Knutson et al., 2015) find a decline in the frequency of events in the Southern Hemisphere, but increasing frequency in the Northern Hemisphere. We therefore examine relationships across all the six TC basins listed in Table 2. The observed TC annual mean numbers for the period 1980-2008 for each basin (Emanuel, 2010) are also listed in Table 2. The North Atlantic makes up a relatively small fraction of the total, with the Pacific dominant in the global locations of tropical cyclones.

3 Results

3.1 The temporal and spatial distribution of GPI and VI

The time series of annual GPI over the 6 TC basins and during the appropriate TC season (The Northern Hemisphere peak TC season is defined to be August through October, and the Southern Hemisphere season is defined to be January through March.)

are shown in Fig. 1. Hereafter, all analyses are calculated and compared using these monthly periods. The mean differences in the TC indices and their component parts are tabulated in Table 3.

The GPI has a rising trend, significant at the 95% level, for all models except BNU-ESM and CanESM2 under RCP4.5, and for all models except CanESM2 and NorESM1-M under G4. Furthermore, the G4 means for all models were significantly lower than their RCP4.5 values. The models we use have considerable range in their absolute values of GPI, which is also a generally observed feature of climate models (Emanuel, 2013). The MIROC-ESM-CHEM model has the largest difference between G4 and RCP4.5 (-16%) while CanESM2 shows the smallest difference (-0.3%). The time series indicate that tropical storms will become more frequent with time and that G4 significantly reduces the numbers.

Fig. 1 also shows the evolution of ventilation index in the TC seasons during 2020 to 2069 among the six models. Note that following the definition of VI in Tang et al. (2014) we use the median value not its mean. During most years from 2020 to 2069, CanESM2, HadGEM2-ES, MIROC-ESM-CHEM and NorESM1-M show the VI under G4 lies above that under RCP45. There are no significant trends throughout the period though all models show slight decreasing trends. Ventilation is disadvantageous for TC genesis. Thus, reducing trends suggest more storms in future, consistent with trends in GPI. As with GPI there is about a factor of 2-3 range in absolute values between the models.

Atmos. Chem. Phys. Discuss., https://doi.org/10.5194/acp-2018-142
Manuscript under review for journal Atmos. Chem. Phys.
Discussion started: 27 March 2018

Fig. 2 shows that the correlations between model differences G4-RCP4.5 for annual GPI and VI. Most models show significant anti-correlation across all TC basins, with the ensemble having significant anti-correlations for all TC basins except South Pacific. The degree of correlation varies widely across the models, with some having coefficients at great as -0.7 and others as low as 0.1. The ensemble mean correlation is only around -0.25, indicating that GPI and VI are addressing sufficiently different aspects of TC to warrant independent analysis.

We next examine the spatial pattern of GPI and VI calculated over the 30-year period: 2040–2069 in the G4 and RCP4.5 experiments. The relative differences as percentages $(GPI_{G4}-GPI_{RCP4.5})/GPI_{RCP4.5}$ during the peak 3-month season of each hemisphere's TC season are shown in Fig. 3. These geographic patterns can be compared with the values in Table 3.

Fig. 3a shows that the GPI anomaly varies by region and by model. For instance, all models except NorESM1-M show negative differences in the North Indian basin. In the Western North Pacific, all models except CanESM2 and HadGEM2-ES show negative differences. Negative differences indicate fewer tropical storms with geoengineering than under greenhouse gas forcing alone. Despite model differences, the ensemble result shows robustly that the GPI difference generally negative in the northern hemisphere but positive in the southern hemisphere. At present the vast majority of tropical storms occur in the northern hemisphere (Table 2), so the overall global numbers would likely decrease.

The spatial distribution of VI also has large variation (Fig. 3b). In the West North Pacific, all models except MIROC-ESM and BNU-ESM have increases, suggesting fewer cyclones in agreement with the results of GPI. All six models have increases in the North Atlantic. In the North Indian Ocean, all models show increasing ventilation index except MIROC-ESM-CHEM and NorESM1-M models, but in the South Indian Ocean, BNU-ESM model shows a decrease, while other models increase. The ensemble results are similar as GPI except for the North Indian basin.

3.2 Accounting for changes in GPI and VI

We use two different methods to examine how the contributing climate variables to GPI and VI account for differences between models and across the TC basins. The objectives are 1) learn which are the key variables in the model simulations of cyclones; 2) find a subset that can be tested against the understanding of how aerosol injection affects the atmosphere heat and water balance and 3) examine if variations in TC basin extent or cyclone seasons may be expected under aerosol injection.

3.2.1 Monthly differences in GPI and VI components between G4 and RCP4.5

To examine the effects of geoengineering on cyclone seasonality, we look at the monthly contributions of the factors that make up GPI and VI. We can express Equation (1) for GPI as the product of four items, respectively representing an atmospheric absolute vorticity item (*AV*), a vertical wind shear item (*WS*), a relative humidity item (*RH*), and an atmospheric potential intensity item (*PI*).

$$GPI = \frac{PI \times RH \times AV}{WS} \tag{5}$$

Where $\mathrm{PI} = \left(\frac{Vpot}{70}\right)^3$, $\mathrm{RH} = \left(\frac{H}{50}\right)^3$, $\mathrm{WS} = (1 + 0.1V_{shear})^2$, $\mathrm{AV} = |10^5\eta|^{\frac{3}{2}}$.

The absolute vorticity and vertical wind shear items can be considered to be dynamic components, while the relative humidity and potential intensity items are thermodynamic ones.

We follow Zhi et.al. (2013) in identifying the individual monthly contributions from the four large-scale environmental processes. First taking the natural logarithm of both sides of Eq. (5), obtains

$$\log(GPI) = \log(PI) + \log(RH) - \log(WS) + \log(AV) \tag{6}$$

And differentiating yields

$$\frac{dGPI}{GPI} = \frac{dPI}{PI} + \frac{dRH}{RH} - \frac{dWS}{WS} + \frac{dAV}{AV} \tag{7}$$

Substituting Eq. (5) into Eq. (7), we have

$$dGPI = dPI \times \frac{RH \times AV}{WS} + dRH \times \frac{PI \times AV}{WS}$$

$$- dWS \times \frac{PI \times RH \times AV}{WS^2} + dAV \times \frac{PI \times RH}{WS} \tag{8}$$

Eq. (8) can be expressed as annual means and monthly anomalies:

$$\delta GPI = \alpha_1 \times \delta PI + \alpha_2 \times \delta RH + \alpha_3 \times \delta WS + \alpha_4 \times \delta AV \tag{9}$$

Where

$$\alpha_1 = \frac{\overline{RH} \times \overline{AV}}{\overline{WS}}$$
$$\alpha_2 = \frac{\overline{PI} \times \overline{AV}}{\overline{WS}}$$
$$\alpha_3 = -\frac{\overline{PI} \times \overline{RH} \times \overline{AV}}{\overline{WS}^2}$$
$$\alpha_4 = \frac{\overline{PI} \times \overline{RH}}{\overline{WS}}$$

And $\delta GPI = GPI - \overline{GPI}$

In Eq. (9), a bar denotes an annual mean value, and δ represents the difference between an individual month and the annual mean, assuming constant coefficients for α_1, α_2, α_3, and α_4.

We are interested in detecting changes between greenhouse gas forcing alone and under geoengineering, so we examine the differences G4-RCP4.5 for each model grouping the TC basins by hemisphere in Fig. 4, and use $\delta GPI_{G4} - \delta GPI_{rcp45}$ to calculate the difference. Fig. 4 clearly shows that *RH* and *WS* make the largest contribution to GPI differences in both hemispheres in all models except MIROC-ESM-CHEM. In the Northern Hemisphere, *RH* and *WS* items show negative contributions in the cyclone season. Hence, these are the factors that enables geoengineering to reduce GPI relative to greenhouse gas forcing. In the Southern Hemisphere there are no clear difference between GPI under G4 or RCP4.5. Absolute vorticity, *AV* makes almost no contribution to the GPI differences under geoengineering in all models.

We also do the same mathematical transform for ventilation index. We obtain annual means and monthly anomalies:

Atmos. Chem. Phys. Discuss., https://doi.org/10.5194/acp-2018-142
Manuscript under review for journal Atmos. Chem. Phys.
Discussion started: 27 March 2018

Atmospheric Chemistry and Physics
Open Access
Discussions

$$\delta \mathrm{VI} = \alpha_5 \delta\left(V_{pot}\right) + \alpha_6 \delta(\chi_m) + \alpha_7 \delta(V_{shear}) \qquad (10)$$

Where $\alpha_5 = -\overline{V_{shear}}\frac{\overline{\chi m}}{\overline{V_{pot}^2}}$ $\alpha_6 = \frac{\overline{V_{shear}}}{\overline{V_{pot}}}$ $\alpha_7 = \frac{\overline{\chi m}}{\overline{V_{pot}}}$

$$\delta \mathrm{VI} = \mathrm{VI} - \overline{VI}$$

Analogously as for GPI, we show also results for VI in Fig. 4. V_{shear} makes the largest contribution to ventilation index differences between geoengineering and greenhouse gas forcing in both hemispheres. Fig. 4 shows that the HadGEM2 values tend to be smaller than for other models and often differ in sign of difference from the other models, consistent with the muted spatial patterns in Fig. 3.

3.2.2 Contributions to GPI and VI across TC basins

The GPI and VI dependencies may be expressed as a regression equation of *X* on *Y* where *Y* is the GPI or VI anomalies under G4 relative to RCP4.5, and the fractional contribution to variance, *S*, of each variable *i* in *X* to *Y* can be written, following Moore et al. (2006) as,

$$S_i = M_i C_i \sigma X_i / \sigma Y \qquad (11)$$

where the σX are the standard deviations of the predictor terms, σY is the standard deviation of the anomalies, *C* are the correlation coefficients of the *X* with *Y*, *M* are the regression coefficients of the *X* with *Y*. The regression can be expressed as a multiple linear regression in log space, and the coefficients simply transformed after fitting. Fitting in log space also allows for the generally heteroscedastic fractional nature of the errors in the variables.

Atmos. Chem. Phys. Discuss., https://doi.org/10.5194/acp-2018-142
Manuscript under review for journal Atmos. Chem. Phys.
Discussion started: 27 March 2018

The relative contributions to GPI anomalies from its four variable items following the regression Eq. (11) are shown in Fig. 5. *RH* is the dominant factor for GPI differences in all models except MIROC-ESM-CHEM and all TC basins. A striking feature of Fig. 5 is that there are very similar patterns of variability between models across all the basins for the *PI* and the *RH* terms, but not for the *WS* and *AV* terms. Fig. 5 also shows that *AV* makes very little contribution to variance explained in the (G4-RCP4.5) differences. For all models except MIROC-ESM-CHEM, *WS* makes about half the contribution to variance explained as *RH*.

Fig. S1 shows the three variables of the ventilation index in a similar way as Fig. 5. V_{shear} makes the largest contribution to VI for all TC basins and all models especially for the BNU-ESM and MIROC-ESM models. Indeed from Fig. S1 it appears that VI may be simply replaced by V_{shear}, but viewing the month by month contributions in Fig. 4 shows that other components are relatively important for some models during some months of the TC season. χ_m has no consistent contribution for the models and basins, and it sometimes make negative contributions to the difference (GPI_{G4}-$GPI_{RCP4.5}$).

The statistical power of a regression equation can be expressed as the F-statistic. Given that the different variables in Figs 5 and S1 show notable differences in their contribution to the GPI and VI, we can use the F-statistic to examine if a reduced model with fewer variables is a better statistical model for the differences under G4 and RCP4.5. GPI has four variables, so there are 15 combination to examine as shown in

Fig. 6. Only for BNU-ESM and MIROC-ESM do the full set of variables have the highest F-statistic. NorESM1-M and MIROC-ESM-CHEM stand out as different from the other models in their general behavior. MIROC-ESM-CHEM is largely governed by *PI* and NorESM1-M by *RH*. In general the models show *RH* has the largest F-statistic for single parameter models, consistent with Figs. 4 and 5. VI has 3 variables, so there are 7 combinations possible. Fig. S2 shows V_{shear} has largest contribution to VI for most of models, and as for GPI, only BNU-ESM and MIROC-ESM models have largest F-statistic for the full set of model variables.

3.3 The key factors affecting TCs

The analysis above shows that *PI* is an important factor affecting TC genesis. According to Eq. (2), V_{pot} is dependent on the static stability of the troposphere, which is related to both sea surface (T_S) and upper tropospheric temperatures (T_O) where rising air flows out of the storm, and which can be represented by tropical tropopause (100 hPa) temperature. Fig. S3 show the correlations across TC basins and seasons for the various fields in RCP4.5 and G4, while Fig. 7 shows the correlations in the differences between G4 and RCP4.5 so that difference made by the geoengineering can be clearly evaluated. Fig. 7a shows the dependence of V_{pot} differences (G4-RCP4.5) on (T_S - T_O) differences for the models. All models have significant correlation for all TC basins except BNU-ESM, which is significant in WNP, ENP, NI and integrated over all TC basins. However, there is an even stronger dependence for V_{pot} on T_S anomalies (Figs. 7b, S3). The model ensemble V_{pot} is better correlated with T_s rather than (T_S - T_O) mostly due to better correlations of NorESM1-M and HadGEM2-ES in Fig. 7b. Fig. S3 shows that correlations for both models under RCP4.5 and G4 separately are not atypical, simply that their (G4-RCP4.5) differences are small. It is also notable that there are worse correlations for the model ensemble values of (T_S - T_O) with V_{pot} under G4 than RCP4.5 (Fig. S3). All models except CanESM2 and NorESM1 show significant correlation between GPI and T_S anomalies shown as Fig. 7c. And all except these two models have significant correlations for all TC basins.

Figs. S4 and S5 show the seasonal variability of T_s and T_0 for all the models. The annual cycle of T_s, is very similar, as expected for all the models, with good agreement on the differences in seasonal cycle between the Northern and Southern Hemispheres. However, for T_0 the models show differences in the shapes and phases of the cycles in both hemispheres, for example only the NorESM1-M model shows roughly antiphase seasonality between the hemispheres. Fig. S6 shows the ERA-interim reanalysis T_0 data, which has similar seasonality in both hemispheres, with peak temperature anomalies in August (~ 1.5°C) and a sharp decline to a long minimum by November or December of similar magnitude. Comparing Figs. S5 and S6 shows that the models generally follow similar patterns under both G4 and RCP4.5, except for NorESM1-M and HadGEM2-ES. HadGEM2-ES is also the model with largest amplitude of seasonal cycle, somewhat larger than in ERA-Interim; other models have smaller amplitudes, with many around half that observed at present. This degree of difference in T_0 simulation likely explains much of the inter-model differences in GPI.

The other common factors across models and basins that affect TCs are relative humidity (H) and vertical wind shear (V_{shear}). In Figs 7d and 7e we plot H and V_{shear} differences between G4 and RCP4.5 as a function of sea surface temperature differences. Relative humidity rises with warming temperatures under both G4 and RCP4.5 (Fig. S3), as expected. But there are obvious differences across the ocean basins with weakest response in ENP, NA and NI and strongest correlations in the Southern Hemisphere basins. Differences G4-RCP4.5 follow a similar spatial pattern, but with a significant anti-correlation in North Atlantic. Across-model differences are larger for correlations of V_{shear} and Ts under both G4 and RCP4.5 (Fig. S3) than for the other key variables. In contrast with the other parameters, there is generally an anti-correlation with T_s across all ocean basins, with the NA basin having the weakest correlations. In terms of the differences in Fig. 7e, all models show clear significant anti-correlations except CanESM2, with the NI and NA basins having weakest correlations. Vecchi et al. (2007) found the tropical Atlantic wind shear increases in model projections under global warming. If the models here capture the effect under G4 and RCP45, we would expect positive correlation between V_{shear} and T_s over the tropical Atlantic for G4 and RCP4.5 in Fig. S3, but all models show negative correlations, although the Pacific Ocean basins more significantly anti-correlated than NA. Li et al. (2010) showed that under warming there is relative shift of towards the central Pacific Ocean of TC genesis away from the North West Pacific. When we plot the G4-RCP4.5 GPI difference map over the Pacific Ocean, we also see a clear anomaly in the Central Pacific (Fig. S7). Li et al. (2010) showed the same effect when using prescribed sea surface temperature patterns from a suite of models, and they account for the changes in TC by surface temperature gradients that drive trade winds, which changes the wind shear. Our result is thus consistent with their findings of changes under greenhouse gas forcing in the Pacific Ocean if the G4 simulation reverses the effects of RCP4.5 effectively.

3.4 The effect of ENSO on GPI

The El Nino-Southern Oscillation (ENSO) is characterized by interannual sea surface temperature (SST) variations in the eastern and central equatorial Pacific Ocean. The impact of ENSO events on the TC activity over the western North Pacific (WNP) has been studied to provide a better understanding of the large-scale steering flow of TCs and the tendency of TC tracks to shift (Wang et al., 2002). There is also clear evidence of teleconnections between ENSO and North Atlantic hurricane season statistics (Gray, 1984; Grinsted et al., 2013). ENSO may be characterized by measures of atmospheric or oceanic variability. We examined the simulated Niño3.4 index of tropical Pacific SSTs in the box 170°W - 120°W, 5°S - 5°N, and the Southern Oscillation Index (SOI) of standardized sea level pressure differences between Tahiti and Darwin, Australia. Previous analysis of the GeoMIP model ENSO response (Gabriel et al., 2015) preferred SST based estimates than noisier atmospheric representations. They also excluded the BNU-ESM, MIROC-ESM and MIROC-ESM-CHEM models from their analysis because of the model's unrealistic amplitudes of ENSO. However, as in the real world, all models and the ensemble we use, show a significant anti-correlation between Niño3.4 index and SOI, except NorESM1-M under

Atmos. Chem. Phys. Discuss., https://doi.org/10.5194/acp-2018-142
Manuscript under review for journal Atmos. Chem. Phys.
Discussion started: 27 March 2018

G4, (Fig. 8). This suggests that while many models, are deficient in aspects of their ENSO variability, they all capture at least some important aspects of ENSO. The correlation coefficients are more significant in RCP4.5 than under G4 for most models. We combined Niño3.4 and SOI indices with equal weighting to get a single representative index of ENSO to compare with GPI and VI.

Annual GPI for the TC basins and the ENSO index during the TC seasons are, in general, significantly correlated under both G4 and RCP4.5 (Fig. 9). The exception being CanESM2 which exhibits anti-correlation between GPI and ENSO index under both G4 and RCP4.5. The analysis for individual basins indicates most models have significant correlations with ENSO in the WNP and the SP basin, except CanESM2 under the G4 experiment, where it is significantly anti-correlated for RCP4.5. BNU-ESM, MIROC-ESM and MIROC-ESM-CHEM have significant correlations in ENP, with NorESM1 and CanESM2 having little or no correlations. Only MIROC-ESM-CHEM has significant correlation between GPI and ENSO in the NA basin, but the R^2 is relatively low, around 0.22. Both BNU-ESM and NorESM1 have significant correlations in the SI basin, while CanESM2 has significant anti-correlation there. So the impact of ENSO is most consistently felt in the Pacific Ocean, with perhaps surprisingly low correlation in the North Atlantic considering the well-known teleconnections with hurricane activity there.

3.5 TC from Track with HadGEM2-ES

As a supplemental analysis to the results based on the GPI and VI, we also employ a widely-used feature tracking software (TRACK vn. 1.4.9) to directly track vorticity maxima that characterize cyclones. Hodges (1995) provides a detailed account of TRACK's core functionality. Jones et al. (2017) also used TRACK to assess geoengineering impact on North Atlantic hurricane statistics, and we follow their approach. Firstly, we determine the relative vorticity (ξ) on the 850, 500, and 250 hPa vertical pressure levels from the zonal (U) and meridional (V) wind using the definition: $\xi = (1/a\times\cos(\theta)) \times (dV/d\lambda - dU\cos(\theta)/d\theta)$, where a is Earth's radius, and θ and λ are the latitude and longitude in radians respectively. U and V are required on 6 hour time steps, but are only available for the HadGEM2-ES model in our ensemble, and limited to the Northern Hemisphere TC season. TRACK detects storms lasting at least 2 days and additionally requires values setting for three parameters. We follow Jones et al. (2017) in selecting: $\xi_1 \geq 4.5$ to express the minimum vorticity intensity required; $\xi_V \geq 3.5$ for the warmth of cyclone core; ξ_1 and ξ_V thresholds must be met for at least 4 consecutive time steps. These criteria represent a relaxation of standard parameters (6, 6, 4) but were tuned to produce a match in the statistics of Atlantic hurricanes contained in the HURDAT2 database (Landsea,et al., 2013) from the HADGEM2-ES historical simulation.

In contrast with Jones et al. (2017) which used data from June through November, we confine the analysis to the Northern Hemisphere TC season (August, September, October). The TRACK results suggest that there are significantly more TC under G4 than with RCP4.5 (Table 4) in all basins except the Eastern North Pacific. This surprising result is not consistent with the changes in GPI and VI for the Northern Hemisphere (Table 3). Table 3 shows that the G4 cools relative to RCP4.5 and that wind shear increases. Furthermore, the TRACK result is not consistent with i) the findings of the statistical model based on surface temperatures (Moore et al., 2015), ii) the proxies (including wind shear) for TC examined by Jones et al. (2017), iii) the statistical-dynamical downscaling CHIPS model of Emanuel (2013). Jones et al. (2017) show that TCs numbers evaluated using the direct counting of storms using the TRACK scheme (Bengtsson et al., 2007) produce much smaller differences between G4 and RCP4.5 than those using statistical downscaling based on either statistical-dynamical downscaling using CHIPS (Emanuel et al., 2004) or simply surface temperatures (Moore et al., 2015).

4 Discussion and Conclusion

Typical ESM are run in coarse-resolution that cannot resolve tropical cyclones and hence do not directly reproduce observed storm intensities and synoptic features related to cyclogenesis (Camargo, 2013). The storms that may be counted using indirect methods such as the TRACK algorithm include the whole climate condition. Statistical methods (Moore et al., 2015) also implicitly include feedbacks between storm and background climate conditions, but dynamical downscaling methods (Emanuel, 2013) cannot include them. The GPI and VI proxies we apply here are useful tools for relating storm activity to meteorological conditions but do not account for changes to TC tracks or intensity. Since they require relatively little data to calculate (monthly means),

Atmos. Chem. Phys. Discuss., https://doi.org/10.5194/acp-2018-142
Manuscript under review for journal Atmos. Chem. Phys.
Discussion started: 27 March 2018

compared with daily or 6 hourly data required for TRACK or the CHIPS tools, and they convey information from more than simply surface temperature fields, they may give reasonable insights into the complex changes to TC under SRM geoengineering schemes.

We evaluated the hurricane index over six TC ocean basins in six CMIP5 and GeoMIP models. We used G4 and RCP4.5 experiments to assess and compare the genesis potential and ventilation indices that diagnose tropical storms in climate models. Based on the climatology of the years 2040-2069, GPI and VI both show small rising trends for TC genesis in all six models under both G4 and RCP4.5 scenarios. Spatial patterns of TCs, show both GPI and VI predicting fewer TC in the North Atlantic and North Indian Ocean under G4 compared with RCP4.5, and more TC in the South Pacific for most models in the ensemble. Thus stratospheric sulphate aerosol injection could lead to fewer TCs in the North Atlantic and Indian Ocean but more TCs in the South Pacific region than under greenhouse gas induced global warming. There is, however, large inter-model variations across the six ocean basins. The impact of ENSO on TCs can be detected in the GPI and shows a rising tendency for GPI under El Niño conditions across the TC basins, especially in the Pacific Ocean.

Detailed statistical analysis of the two TC indices indicates that the thermodynamic variables potential intensity and relative humidity are the dominant ones affecting genesis potential, while the dynamic variables such as absolute vorticity and entropy deficit are much less important. Vertical wind shear is a dynamic variable and dominates the ventilation index. By examining the contributions of variables to differences in GPI and VI under geoengineering and greenhouse gas forced climates we show that relative humidity is the dominant factor for GPI differences in all models and all TC basins, except MIROC-ESM-CHEM for which potential intensity is the dominant factor. The analysis suggests that a simplified representation of TCs depending on fewer variables is possible, but does require analysis of particular model behavior before choosing those variables. Although wind shear is important and a dynamic variable, it in encouraging that the thermodynamic state of the system is of prime importance for the GPI, suggesting that statistical methods of predicting changes in hurricane and storm behavior are plausible. But, these indices cannot fully represent the actual TC variations due to the complexity of TC genesis and evolution.

Potential intensity is related to the difference between sea surface temperature and outflow temperature (the 100 hPa level). In fact we note that SSTs alone provide a better correlation with both potential intensity and GPI. This result is similar with previous observational (Grinsted et al., 2013) and modeling (Wu and Lau, 1992) studies that suggest it is the geographical distribution of SST anomalies that are crucial for the development of TC. Recent analysis of GeoMIP results by Davis et al. (2016), on the extent of the tropical belt under G1 and 4×CO2 experiments, demonstrates that tropical upper-tropospheric temperature changes are well-correlated with the change in global-mean surface temperature. This is because changes in the static stability characterized by upper troposphere and surface temperature differences scales with the moist adiabatic lapse rate and surface temperatures. In contrast with the solar dimming G1

Atmos. Chem. Phys. Discuss., https://doi.org/10.5194/acp-2018-142
Manuscript under review for journal Atmos. Chem. Phys.
Discussion started: 27 March 2018

experiments analyzed by Davis et al., (2016), here we analysis G4 which is an aerosol injection scheme. The aerosol heats the stratosphere mainly between the 16-25 km elevation injection levels with warming at the tropopause of about 0.6 °C relative to RCP4.5 for the MIROC-ESM-CHEM model (Pitari et al., 2014). This is about half the range of the G4-RCP4.5 difference in static stability (Fig. 7). Hence, we would expect to see a significant improvement in correlation of potential intensity and GPI by using 100 hPa temperatures in addition to SSTs, but we do not. Table 3 shows that the upper troposphere measured by T_0 does not warm with most models under G4, which is consistent with the impact of G1 on the troposphere. The result is that the models used here have a better relationship with sea surface temperatures than static stability, and suggests that the aerosol heating effects are not influencing simulated TC genesis.

The change in relative humidity on the tropical ocean basins in future is a key aspect of TC genesis according to our analysis. Models tend to agree on the sign of change in relative humidity as temperatures rise, but there are consistent differences in strength of response across the ocean basins. The differences in response (G4-RCP4.5) even indicate a difference in sign of North Atlantic response under geoengineering from the other basins. This indicates that although relative humidity is important for most models, changes in TC genesis processes between basins affect its utility as a predictor variable. The final variable, vertical wind shear, shows large scatter across the models, but consistent anti-correlation between V_{shear} and surface temperature, and that relationship is somewhat stronger under G4 than RCP4.5. The changes in GPI over the Pacific

Atmos. Chem. Phys. Discuss., https://doi.org/10.5194/acp-2018-142
Manuscript under review for journal Atmos. Chem. Phys.
Discussion started: 27 March 2018

Atmospheric Chemistry and Physics Discussions
Open Access
EGU

Ocean under G4 compared with RCP4.5 are similar to previous results comparing patterns of TC genesis under 20th century surface temperatures relative to 21st patterns (Li et al., 2010). Overall our analysis of the driving parameters in GPI, suggests that despite large model differences, the simple dependence of GPI on surface temperatures is reasonably robust.

Smyth et al. (2017) report the seasonal migration of the Intertropical Convergence Zone (ITCZ) in G1, associated with preferential cooling of the summer hemisphere, and annual mean ITCZ shifts in some models that are correlated with the warming of one hemisphere relative to the other. ITCZ location is correlated with tropical cyclone and season. Our analysis of seasonality of TCs shows that there appears to be a difference in behavior between the Southern and Northern Hemispheres, with the southern one showing no consistent changes between models under RCP4.5 and G4 scenarios. Davis et al. (2016) show that there are differences in the evolution of the northern and southern Hadley cells under greenhouse forcing, with the expansion of the northern one scaling non-linearly with temperature. Differences seem to be driven fundamentally by the equator-pole temperature gradient, and therefore may be expected given the far larger polar amplification in the Northern compared with Southern Hemisphere.

Many models, owing to their low resolutions, produce much weaker and larger TCs (Camargo et al., 2005) than seen observationally. Considering the insufficient resolution of most models, evaluating the GPI and VI may be a better diagnostic of TC variations under different climates. The results presented here suggest that SRM produces reductions in TCs across most of the major storm basins, and would be primarily due to reduced sea surface temperatures in the genesis regions.

Acknowledgements. We thank the climate modeling groups for participating in the Geoengineering Model Intercomparison Project and their model development teams; the CLIVAR/WCRP Working Group on Coupled Modeling for endorsing the GeoMIP; and the scientists managing the earth system grid data nodes who have assisted with making GeoMIP output available. This research was funded by the National Basic Research Program of China (Grant 2015CB953600) and the Fundamental Research Funds for the Central Universities (312231103).

Atmos. Chem. Phys. Discuss., https://doi.org/10.5194/acp-2018-142
Manuscript under review for journal Atmos. Chem. Phys.
Discussion started: 27 March 2018

REFERENCES

Balaguru, K., Foltz, G. R., Leung, L. R., Asaro, E. D’ , Emanuel, K. A., H. Liu, and Zedler, S. E.: Dynamic Potential Intensity: An improved representation of the ocean’s impact on tropical cyclones, Geophys. Res. Lett., 42, 6739-6746, 2015.

Bengtsson, L., Hodges, K. I. and Esch, M.: Tropical cyclones in a T159 resolution global climate model: comparison with observations and re-analyses, Tellus A, 59: 396–416, 2007.

Bentsen, M., Bethke, I., Debernard, J. B., Iversen, T., Kirkevåg, A., Seland, Ø., Drange, H., Roelandt, C., Seierstad, I. A., Hoose, C., and Kristjánsson, J. E.: The Norwegian Earth System Model, NorESM1-M – Part 1: Description and basic evaluation of the physical climate, Geosci. Model Dev., 6, 687–720, 2013.

Bister, M., and Emanuel, K. A.: The genesis of Hurricane Guillermo: TEXMEX analyses and a modeling study, Mon. Wea. Rev., 125, 2662–2682, 1997.

Bister, M., and Emanuel, K. A.: Dissipative heating and hurricane intensity, Meteor. Atmos. Phys., 65, 233–240, 1998.

Camargo, S. J., Barnston, A. G., and Zebiak, S. E.: A statistical assessment of tropical cyclone activity in atmospheric general circulation models, Tellus A, 57, 589-604, 2005.

Camargo, S. J.: Global and regional aspects of tropical cyclone activity in the CMIP5 models. J. Clim., 26, 9880–9902, 2013.

Chan, J. C. L.: Interannual and interdecadal variations of tropical cyclone activity over the western North Pacific, Meteor. Atmos. Phys., 89, 143-152, 2005.

Chylek, P., Li, J., Dubey, M. K., Wang, M., and Lesins, G.: Observed and model simulated 20th century Arctic temperature variability: Canadian Earth System Model CanESM2.Atmos, Chem. Phys. Discuss., 11, 22 893–22 907, 2011.

Crutzen, P. J.: Albedo enhancement by stratospheric sulfur injections: A contribution to resolve a policy dilemma?, Clim. Change, 77(3), 211–220, 2006.

Collins, W. J., Bellouin, N., Doutriaux-Boucher, M., Gedney, N., Halloran, P., Hinton, T., Hughes, J., Jones, C. D., Joshi, M., Liddicoat, S., Martin, G., O’Connor, F., Rae, J., Senior, C., Sitch, S., Totterdell, I., Wiltshire, A., and Woodward, S.: Development and evaluation of an Earth-System model – HadGEM2, Geosci. Model Dev., 4, 1051–1075, 2011.

Davis, N. A., Seidel, D. J., Birner, T., Davis, S. M., and Tilmes, S.: Changes in the width of the tropical belt due to simple radiative forcing changes in the GeoMIP simulations, Atmos. Chem. Phys., 16, 10083-10095, 2016.

Atmos. Chem. Phys. Discuss., https://doi.org/10.5194/acp-2018-142
Manuscript under review for journal Atmos. Chem. Phys.
Discussion started: 27 March 2018

Atmospheric Chemistry and Physics
Open Access
Discussions

Emanuel, K. A.: Tropical cyclone activity downscaled from NOAA-CIRES reanalysis, Journal of Advances in Modeling Earth Systems, 2:1–12, 1908-1958, 2010.

Emanuel, K. A.: Downscaling CMIP5 climate models shows increased tropical cyclone activity over the 21st century, PNAS, 110(30), 12219-12224, 2013.

Emanuel, K. A.: A statistical analysis of tropical cyclone intensity, Mon. Wea. Rev., 128, 1139–1152, 2000.

Emanuel, K. A.: Atmospheric Convection, Oxford University Press, 580 pp, 1994.

Emanuel, K. A., Nolan, D.: Tropical cyclone activity and global climate system, Am. Meteorol. Soc., 26, 240–241, 2004.

Emanuel, K. A., Sundararajan, R., and Williams, J.: Hurricanes and global warming: Results from downscaling IPCC AR4 simulations, Bull. Amer. Meteor. Soc., 89, 347-367, 2008.

Emanuel, K. A.: Climate and tropical cyclone activity: A new model downscaling approach, J. Climate, 19, 4797-4802, 2006.

Gabriel, C. J. and Robock, A.: Stratospheric geoengineering impacts on El Niño/Southern Oscillation, Atmos. Chem. Phys., 15, 11949-11966, 2015.

Gray, W. M.: Hurricanes: Their formation, structure, and likely role in the tropical circulation, Roy. Meteor. Soc., 155-218, 1979.

Gray, W. M.: Atlantic seasonal hurricane frequency: Part I: El Niño and 30 mb quasi-biennial oscillation influences, Mon. Wea. Rev., 112, 1649-1668, 1984.

Grinsted, A., Moore, J. C., Jevrejeva, S.: A homogeneous record of Atlantic hurricane surge threat since 1923, PNAS, 109(48):19601-19605, 2012.

Grinsted, A., Moore, J. C., Jevrejeva, S.: Projected Atlantic tropical cyclone threat from rising temperatures, PNAS, 110(14), 5369-5373, 2013.

Huneeus, N., Boucher, O., Alterskj, K., Cole, J. N. S., Curry, C. L., Ji, D., Jones, A., Kravitz, B., Kristjánsson, J. E., Moore, J. C., Muri, H., Niemeier, U., Rasch, P., Robock, A., Singh, B., Schmidt, H., Schulz, M., Tilmes, S., Watanabe, S., and Yoon, J.-H.: Forcings and feedbacks in the GeoMIP ensemble for a reduction in solar irradiance and increase in CO2, J. Geophys. Res. Atmos., 119, 5226–5239, 2014.

Hodges, K.: Feature tracking on a unit sphere, Mon. Wea. Rev., 123, 3458–3465,1995.

IPCC: Climate Change 2007: Synthesis Report. Contribution of Working Groups I, II and III to the Fourth Assessment Report of the Intergovernmental Panel on Climate

Atmos. Chem. Phys. Discuss., https://doi.org/10.5194/acp-2018-142
Manuscript under review for journal Atmos. Chem. Phys.
Discussion started: 27 March 2018

Change, edited by Core Writing Team, R. K. Pachauri, and A. Reisinger, 104 pp., IPCC, Geneva, Switzerland, 2007.

Ji, D., Wang, L., Feng, J., Wu, Q., Cheng, H., Zhang, Q., Yang, J., Dong, W., Dai, Y., Gong, D., Zhang, R.-H., Wang, X., Liu, J., Moore, J. C., Chen, D., and Zhou, M.: Description and basic evaluation of Beijing Normal University Earth System Model(BNU-ESM) version 1, Geosci. Model Dev., 7, 2039–2064, 2014.

Jones, A. C., Haywood, J. M., Dunstone, N., Emanuel, K., Hawcroft, M. K., Hodges, K. I., Jones, A.: Impacts of hemispheric solar geoengineering on tropical cyclone frequency, Nat. Commun., 8 (1382), 1-10, 2017.

Kravitz, B., Robock, A., Boucher, O., Schmidt, H., Taylor, K. E., Stenchikov, G., and Schulz, M.: The Geoengineering Model Intercomparison Project (GeoMIP), Atmos. Sci. Lett., 12, 162-167, 2011a.

Kravitz, B., Robock, A., Tilmes, S., Boucher, O., English, J. M., Irvine, P. J., Jones, A., Lawrence, M. G., MacCracken, M., Muri, H., Moore, J. C., Niemeier, U., Phipps, S. J., Sillmann, J., Storelvmo, T., Wang, H., and Watanabe, S.: The Geoengineering Model Intercomparison Project Phase 6 (GeoMIP6): simulation design and preliminary results, Geosci. Model Dev., 8, 3379-3392, 2015.

Kang, N. and Elsner, J. B.: Consensus on Climate Trends in Western North Pacific Tropical Cyclones, J. Climate, 25, 7564–7573, 2012.

Knutson, T. R., Sirutis, J., Zhao, M., Tuleya, R., Bender, M., Vecchi, G., Villarini, G., and Chavas, D.: Global projections of intense tropical cyclone activity for the late twenty-first century from dynamical downscaling of CMIP5/RCP4.5 scenarios, J. Climate, 28, 7203–7224, 2015.

Landsea, C. W.: Hurricanes and global warming, Nature, 438, E11-E12, 2005.

Landsea, C. W., Franklin, J. L.: Atlantic hurricane database uncertainty and presentation of a new database format, Mon. Weather Rev., 141, 3576–3592, 2013.

Li, T., Kwon, M., Zhao, M., Kug, J. ‐ S., Luo, J. ‐ J, and Yu, W.: Global warming shifts Pacific tropical cyclone location, Geophys. Res. Lett., 37, L21804, 2010.

Moore, J. C., Kekonen, T., Grinsted, A., and Isaksson, E.: Sulfate source inventories from a Svalbard ice core record spanning the Industrial Revolution, J. Geophys. Res., 111, D15307, 2006.

Moore, J. C., Grinsted, A., Guo, X., Yu, X., Jevrejeva, S., Rinke, A., Cui, X., Kravitz, B., Lenton, A., Watanabe, S., Ji, D.: Atlantic hurricane surge response to geoengineering, PNAS, 112 (45), 13794-13799, 2015.

Nolan, D. S.: What is the trigger for tropical cyclogenesis?, Aust. Meteorol. Mag., 56, 241-266, 2007.

Pitari, G., Aquila, V., Kravitz, B., Robock, A., Watanabe, S., Cionni, I., Luca N. D., Genova, G.D., Mancini, E., and Tilmes, S.: Stratospheric ozone response to sulfate geoengineering: Results from the Geoengineering Model Intercomparison Project (GeoMIP), J. Geophys. Res. Atmos., 119, 2629–2653, 2014.

Rappin, E. D., Nolan, D. S., and Emanuel, K. A.: Thermodynamic control of tropical cyclogenesis in environments of radiative convective equilibrium with shear, Q. J. R. Meteorol. Soc., 136, 1954-1971, 2010.

Rogelj, J., Luderer, G., Pietzcker, R.C., Kriegler, E., Schaeffer, M., Krey, V., Riahi, K.: Energy system transformations for limiting end-of-century warming to below 1.5° C, Nature Climate Change, 5, 519-527, 2015.

Smyth, J. E., Russotto, R. D., and Storelvmo, T.: Thermodynamic and dynamic responses of the hydrological cycle to solar dimming, Atmos, Chem. Phys., 17, 6439-6453, 2017.

Song, Y. J., Wang, L., Lei, X. Y., and Wang, X. D.: Tropical cyclone genesis potential index over the western North Pacific simulated by CMIP5 models, Adv. Atmos. Sci., 32(11), 1539-1550, 2015.

Tang, B., and Emanuel, K. A.: A ventilation index for tropical cyclones, Bull. Am. Meteorol. Soc., 93, 1901-1912, 2012a.

Tang, B., and Camargo, S. J.: Environmental control of tropical cyclones in CMIP5: A ventilation perspective, J. Adv. Model. Earth Syst., 6, 115-128, 2014.

Taylor, K. E., Stouffer, R. J., and Meehl, G. A.: An overview of CMIP5 and the experiment design, Bull. Amer. Meteor. Soc., 93, 485-498, 2012.

Tippett, M. K., Camargo, S. J., and Sobel, A. H.: A Poisson regression index for tropical cyclone genesis and the role of large-scale vorticity in genesis, J. Climate, 24, 2335–2357, 2011.

Tory, K.J., Chand, S.S., McBride, J.L., Ye, H., and Dare, R.A.: Projected Changes in Late-Twenty-First-Century Tropical Cyclone Frequency in 13 Coupled Climate Models from Phase 5 of the Coupled Model Intercomparison Project, J. Climate, 26, 9946–9959, 2013.

Vecchi, G. A., and Soden, B. J.: Increased tropical Atlantic wind shear in model projections of global warming, Geophys. Res. Lett., 34, L08702, 2007.

Wang, B. and Chan, J. C.: How Strong ENSO Events Affect Tropical Storm Activity over the Western North Pacific, J. Climate, 15, 1643–1658, 2002.

Atmos. Chem. Phys. Discuss., https://doi.org/10.5194/acp-2018-142
Manuscript under review for journal Atmos. Chem. Phys.
Discussion started: 27 March 2018

Atmospheric Chemistry and Physics
Discussions
Open Access

Wang, X., Zhou, W., Li, C. Y., and Wang, D. X.: Effects of the East Asian summer monsoon on tropical cyclone genesis over the South China Sea on an interdecadal timescales, Adv. Atmos. Sci., 29, 249-262, 2012.

Watanabe, S., Hajima, T., Sudo, K., Nagashima, T., Takemura, T., Okajima, H., Nozawa, T., Kawase, H., Abe, M., Yokohata, T., Ise, T., Sato, H., Kato, E., Takata, K., Emori, S., and Kawamiya, M.: MIROC-ESM 2010: model description and basic results of CMIP5-20c3m experiments, Geosci. Model Dev., 4, 845-872, 2011.

Wigley, T. M. L.: A combined mitigation/geoengineering approach to climate stabilization, Science, 314(5798), 452-454, 2006.

Wu, G., and Lau, N.-C.: A GCM simulation of the relationship between tropical-storm formation and ENSO, Mon.Wea.Rev.,120,958-977, 1992.

Yu, X., Moore, J.C., Cui, X., Rinke, A., Ji, D., Kravitz, B., Yoon, J.-H.: Impacts, effectiveness and regional inequalities of the GeoMIP G1 to G4 solar radiation management scenarios, Global Planet Change, 129, 10-22, 2015.

Zhi, L., Yu, W., Li, T., Murty, V.S. and Tangang F.: Bimodal Character of Cyclone Climatology in the Bay of Bengal Modulated by Monsoon Seasonal Cycle, J. Climate, 26, 1033–1046, 2013.

Atmos. Chem. Phys. Discuss., https://doi.org/10.5194/acp-2018-142
Manuscript under review for journal Atmos. Chem. Phys.
Discussion started: 27 March 2018

Atmospheric Chemistry and Physics
Discussions
Open Access
EGU

Tables and Figures

Table 1. Climate models used in this study

Model	Reference	Resolution (Lon×Lat)	ensemble members
BNU-ESM	Ji et al. (2014)	128×64	1
CanESM2	Chylek et al. (2011)	128×64	3
HadGEM2-ES	Collins et al.(2011)	192×144	3
MIROC-ESM	Watanabe et al. (2011)	128×64	1
MIROC-ESM-CHEM	Watanabe et al. (2011)	128×64	9
NorESM1-M	Bentsen et al. (2013)	144×96	1

Table 2. Definitions of Regions and numbers of observed TC

Region	Latitudes	Longitudes	Annual Mean Numbers and percentages (1980-2008)
North Atlantic (NA)	6-18°N	20-60°W	12 (15%)
Eastern North Pacific (ENP)	5-16°N	90-170°W	15 (19%)
Western North Pacific (WNP)	5-20°N	110-150°E	25 (32%)
North Indian (NI)	5-20°N	50-110°E	4 (5%)
South Indian (SI)	5-20°S	50-100°E	23 (29%)
South Pacific (SP)	5-20°S	160E-130°W	

Table 3. Differences (G4-RCP4.5) in TC basins and season during 2040-2069 year calculated point-by-point. Northern Hemisphere numbers are above and Southern Hemisphere below Bold fonts are significant at 95% level. The ensemble means are not normalized

Models	*Ts* (°C)	*To* (°C)	*Ts-To* (°C)	GPI	V_{pot} (ms^{-1})	*H* (%)	V_{shear} (ms^{-1})	η ($\times 10^{-8}$ s^{-1})	VI ($\times 10^{3}$)	χ_m ($\times 10^{3}$)
BNU-ESM	**-0.51**	0.023	-0.53	-0.62	-0.59	-0.26	0.012	-1.2	20	17
	-0.43	-0.044	-0.38	0.057	-0.040	0.73	0.076	0.83	7.2	19
MIROC-ESM	-0.32	-0.52	0.20	-0.50	-1.0	-0.28	0.28	1.3	15	-4.9
	-0.24	-0.52	0.28	0.0027	-0.28	0.12	-0.16	-0.32	1.6	8.6
MIROC-ESM-CHEM	**-0.29**	-0.50	0.27	**-2.6**	**6.62**	**4.6**	**1.9**	0.56	8.7	-11
	-0.24	-0.48	0.29	0.19	**6.34**	**3.5**	**2.3**	-0.76	-5.8	1.2
CanESM2	**-0.50**	-0.13	-0.37	-0.017	-0.86	0.17	-0.045	-0.08	13	19
	-0.46	-0.086	-0.37	-0.044	-0.44	-0.21	0.026	-5.3	-2.7	4.9
NorESM1-M	-0.27	-0.13	-0.15	-2.7	-1.0	-0.24	0.33	-3.7	19	2.8
	-0.24	-0.14	-0.095	1.9	-0.65	-0.52	0.085	-1.9	-21	-9.8
HadGEM2-ES	**-0.75**	0.13	-0.88	-0.30	-1.2	0.43	0.083	5.8	23	52
	-0.70	0.075	-0.73	0.053	-0.66	-0.018	-0.028	1.7	3.4	37
Ensemble	**-0.44**	-0.17	**-0.24**	-1.1	**0.33**	0.73	0.43	0.44	16	12
	-0.38	-0.20	-0.17	0.38	0.71	0.60	0.38	-0.98	-3.0	10

Atmos. Chem. Phys. Discuss., https://doi.org/10.5194/acp-2018-142
Manuscript under review for journal Atmos. Chem. Phys.
Discussion started: 27 March 2018

Table 4. Mean TC frequency in Northern Hemisphere basins from the 3-member ensemble of HadGEM2-ES using TRACK (4.5, 3.5, 4) during August, September, October 2020-2069. Bold indicates regions with significantly more TC under G4 than RCP4.5 at the 95% level.

Region	Mean G4	St.Dev G4	Mean RCP4.5	St.Dev RCP4.5
WNP	**5.0**	**2.0**	**4.4**	**1.8**
ENP	11.5	3.4	11.7	3.3
NA	**1.2**	**1.0**	**0.8**	**0.8**
NI	**3.5**	**1.5**	**3.0**	**1.7**

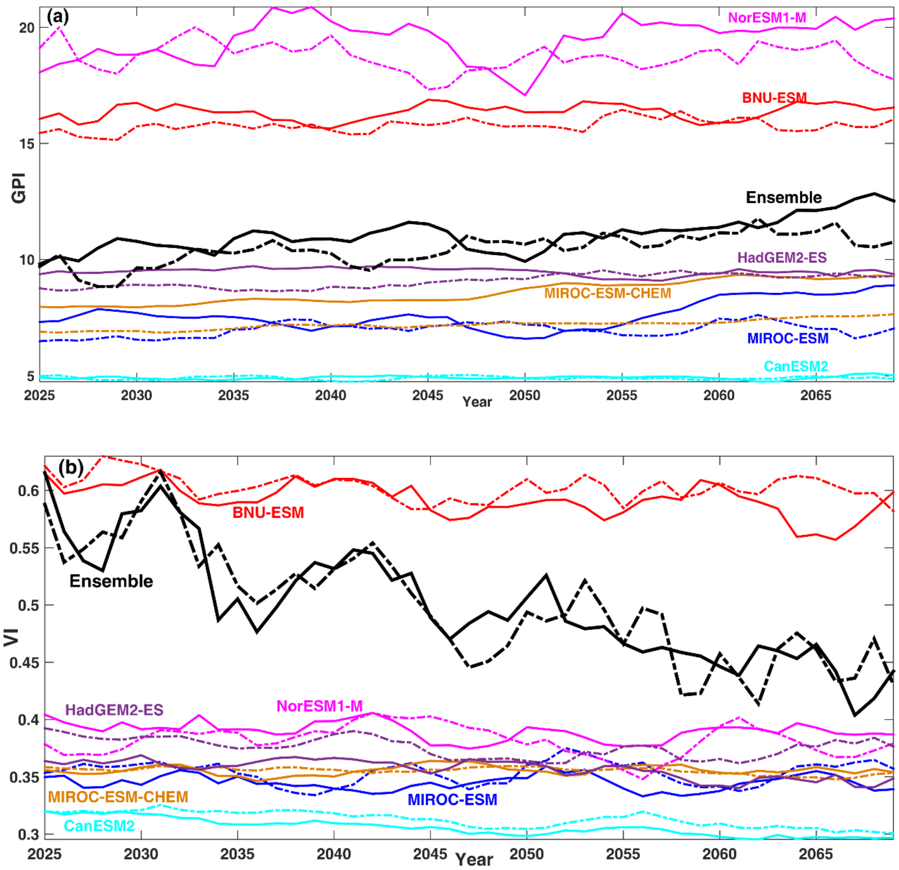

Figure 1. Five yearly moving annual averages, of (a) GPI index and (b) ventilation index in TC season and TC basin. Solid lines denote forcing under RCP4.5 and dotted lines values under G4. Ensemble mean series were calculate using normalized time series, shifted by the ensemble mean.

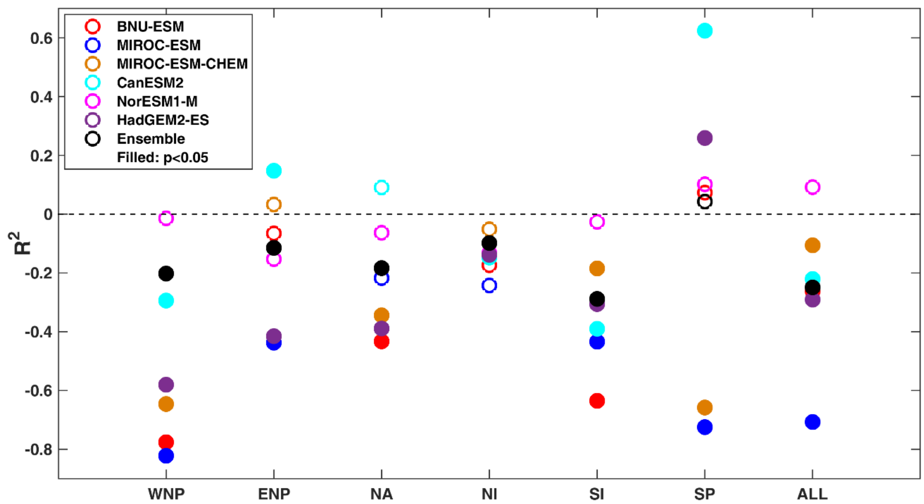

Figure 2. The correlation coefficients (R^2) between annual GPI and VI anomalies (G4-RCP4.5) during TC season and six ocean TC basins. The MIROC-ESM-CHEM model has 9 ensemble members, the CanESM2 model has 3 ensemble members, and other models have one member. Each model is weighted equally and normalized for the ensemble regardless of the number of separate realizations. Dashed line represent R^2=0.

Atmos. Chem. Phys. Discuss., https://doi.org/10.5194/acp-2018-142
Manuscript under review for journal Atmos. Chem. Phys.
Discussion started: 27 March 2018

Atmospheric Chemistry and Physics
Open Access
Discussions

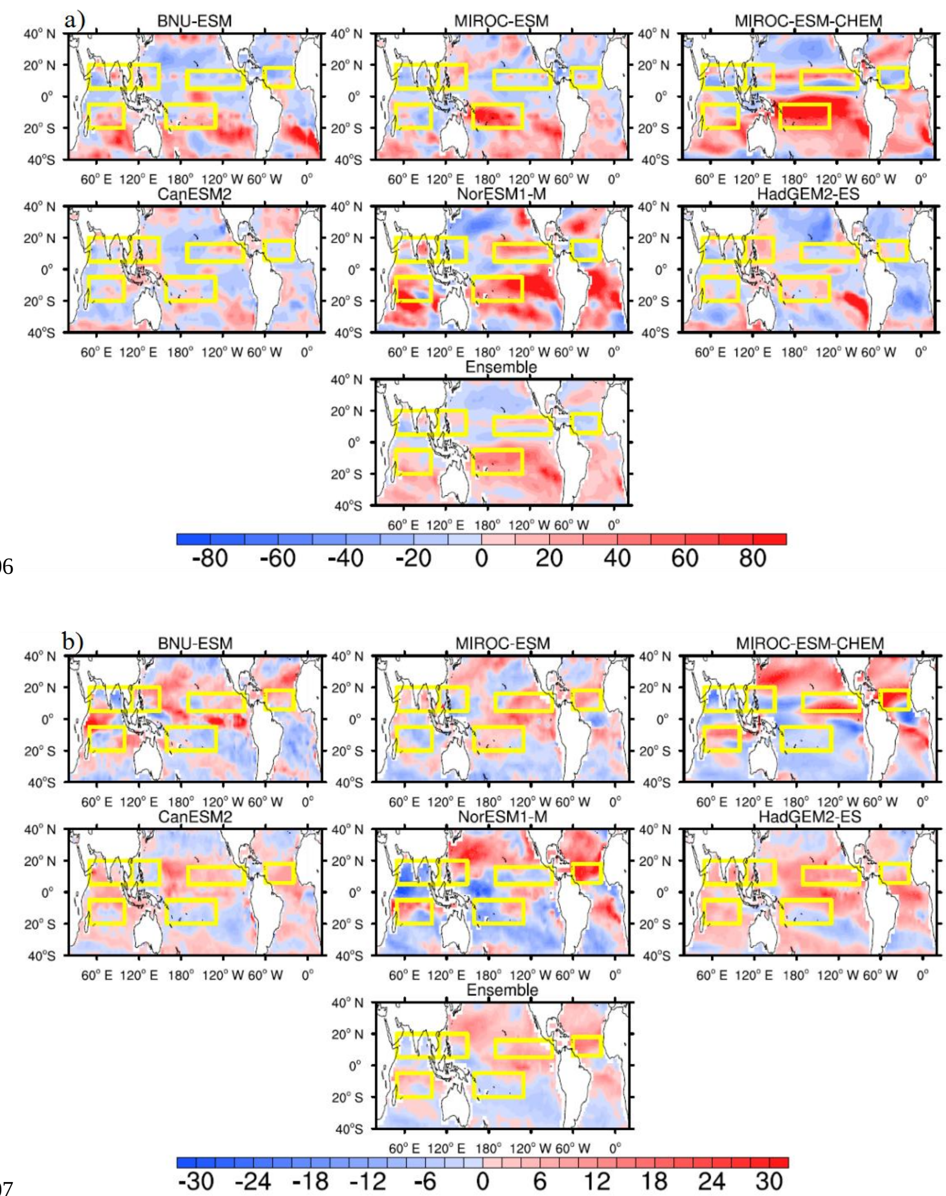

Figure 3. Spatial distribution at each grid point during the appropriate TC season between 2040-2069 of the anomaly (GPI_{G4}-$GPI_{RCP4.5}$)/$GPI_{RCP4.5}$ as a percentage, for a) GPI and b) VI. Yellow rectangles delimit the six TC ocean basins. The Northern

Hemisphere peak TC season is defined to be August through October, and the Southern Hemisphere season is defined to be January through March.

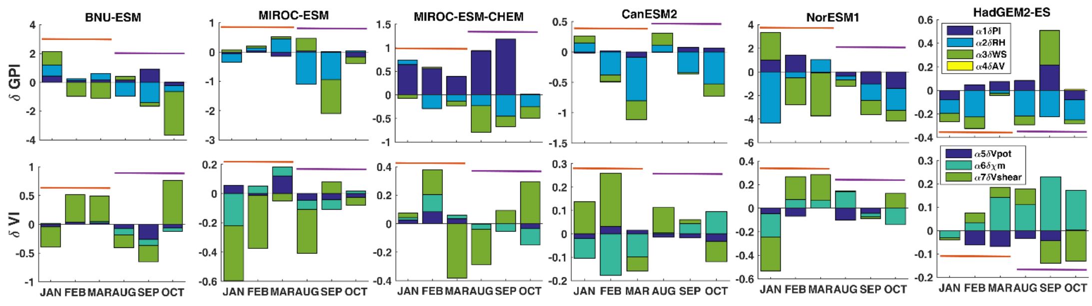

Figure 4 The mean month contribution of each variable to the difference (G4-RCP4.5) for the years 2040-2069 in TC basins and TC season in GPI and VI. Brown lines represent Southern Hemisphere and purple lines represent Northern Hemisphere TC seasons.

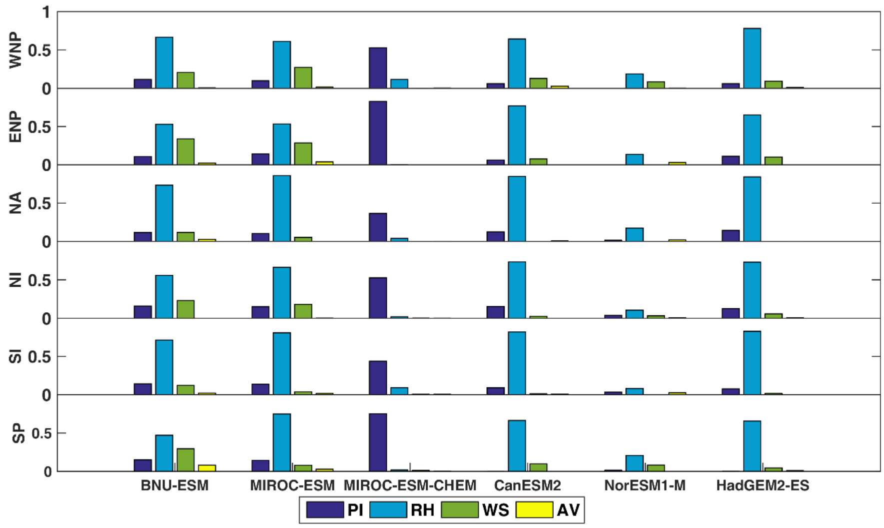

Figure 5. The fractional variance contribution of components of GPI during the TC season and within the six TC basins during 2040-2069.

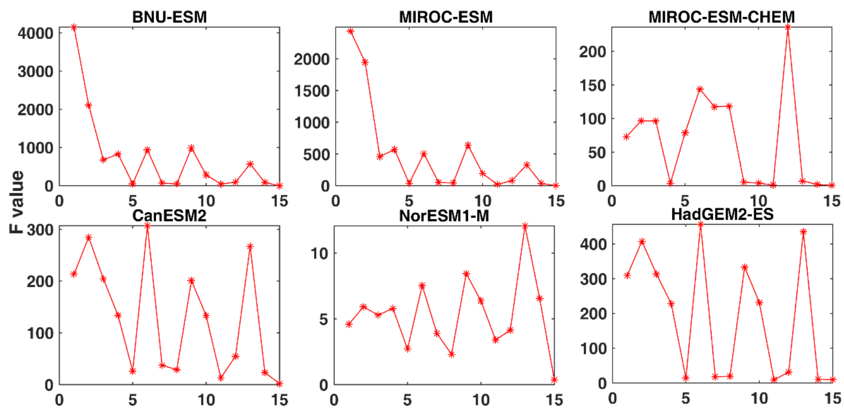

Figure 6. The F-statistic of the 15 different combinations of regression variables for GPI differences between G4 and RCP4.5. The x-axis on each panel represents the combination of components used as predictors in each regression equation: 1:*(PI,RH,WS,AV)*, 2:*(PI,RH,WS)*, 3:*(PI,RH,AV)*, 4:*(AV,RH,WS)*, 5:*(PI,AV,WS)*,

Atmos. Chem. Phys. Discuss., https://doi.org/10.5194/acp-2018-142
Manuscript under review for journal Atmos. Chem. Phys.
Discussion started: 27 March 2018

6:*(PI,RH)*, 7:*(PI,WS)*, 8:*(PI,AV)*, 9:*(RH,WS)*, 10:*(RH,AV)*, 11:*(AV,WS)*, 12:*(PI)*, 13:*(RH)*, 14:*(WS)*, 15:*(AV)*.

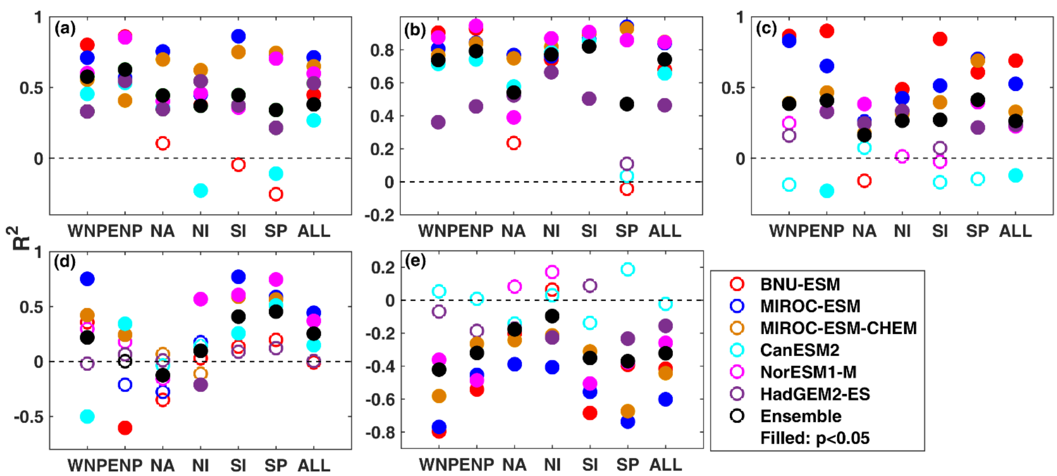

Figure 7. The correlations (R^2) between differences (G4-RCP4.5) during TC season and across the six TC basins for the years 2040-2069 for (a) V_{pot} anomalies as a function static stability $T_S - T_O$. Panels b-e show R^2 coefficients for anomalies with sea surface temperature differences (T_s) and: (b) V_{pot}, (c) GPI , (d) relative humidity, (e) vertical wind shear. Each model is weighted equally in the ensembles regardless of number of observations.

Atmos. Chem. Phys. Discuss., https://doi.org/10.5194/acp-2018-142
Manuscript under review for journal Atmos. Chem. Phys.
Discussion started: 27 March 2018

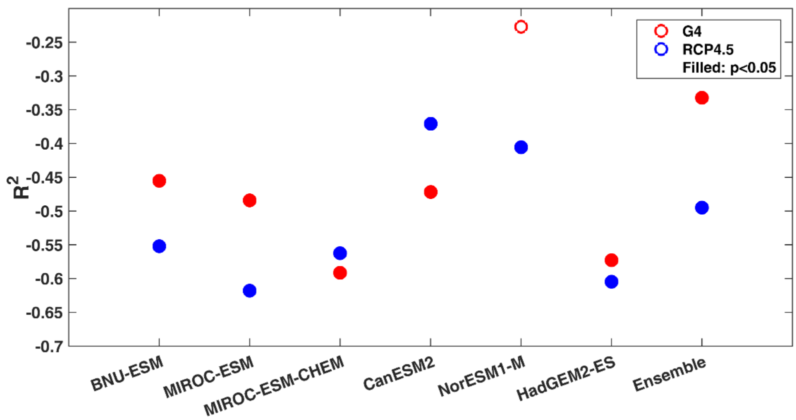

Figure 8. The model correlation coefficients between annual Niño3.4 index and SOI during TC season for 2040-2069.

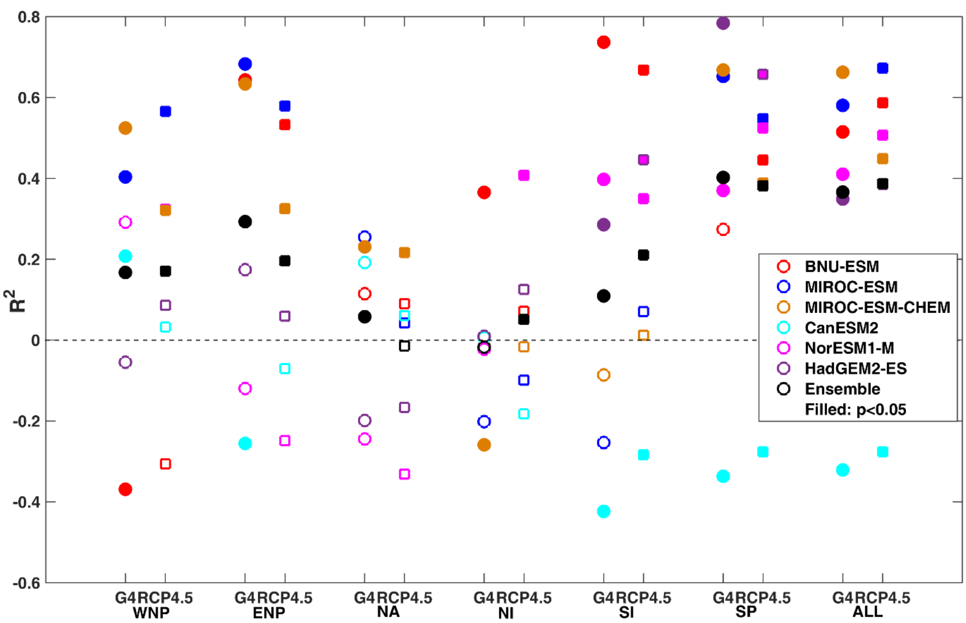

Figure 9. The correlation of GPI as a function of (Niño3.4-SOI)/2 during TC season and six TC basins and all TC basins for the G4 and RCP4.5 experiments.